Carbohydrate Polymers 93 (2013) 731–739

Contents lists available at SciVerse ScienceDirect

Carbohydrate Polymers

journal homepage: www.elsevier.com/locate/carbpol

In situ synthesized novel biocompatible titania–chitosan nanocomposites with high surface area and antibacterial activity

K. Kavitha[a], S. Sutha[a], M. Prabhu[a], V. Rajendran[a,*], T. Jayakumar[b]

[a] *Centre for Nano Science and Technology, K. S. Rangasamy College of Technology, K.S.R. Kalvi Nagar, Tiruchengode-637 215, Namakkal (Dt.), Tamil Nadu, India*
[b] *Metallurgy and Materials Department, Indira Gandhi Centre for Atomic Research, Kalpakkam 603102, Tamil Nadu, India*

ARTICLE INFO

Article history:
Received 17 October 2012
Received in revised form
12 December 2012
Accepted 14 December 2012
Available online 7 January 2013

Keywords:
Titania–chitosan
Nanocomposite
Cytotoxicity
Biocompatibility
Antibacterial activity
Surface area

ABSTRACT

A series of titania–chitosan nanocomposites (2:*x* (0.12, 0.25, 0.5, 1.0 and 2.0 g)) were synthesized using *in situ* sol–gel method and comprehensively characterized using conventional techniques. The resultant particles showed anatase phase, spherical and irregular morphology with particle size of 4.5–10.5 nm. Nanocomposites with higher surface area (114–265 m^2/g) and high purity were obtained. The characterized samples were analyzed in 1.5 mM simulated body fluid (1.5 SBF) and human gastric adenocarcinoma cell line to explore the bioactivity and biocompatibility. Antibacterial activity against *Staphylococcus aureus* was also evaluated. The formation of apatite layer on 1.5 SBF-immersed samples confirms the bioactivity of all the nanocomposites. High surface area, appropriate hydroxyapatite formation, specific antibacterial action, increased cell viability, controlled swelling and degrading rate are favorably achieved at 2:1 nanocomposite ratio. This study shows titania–chitosan nanocomposites as the promising biomaterial for orthopedic and tissue engineering applications.

1. Introduction

Bone tissue engineering and orthopedics are emerging areas of biomaterial science that aim to improve the osseointegration, mimic the natural process to repair and maintain the function of the bone using effective biomaterials (Isikli, Hasirci, & Hasirci, 2012; Zhang & Zhang, 2004). Nano-titania (TiO_2) is an effective biological material used widely in biomedical research because of its unique physiochemical nature (Hua, Cheuk, Wei-ning, Chen, & Chang-fa, 2007), and it accelerates the formation of bone-like apatite through the Ti–OH site. TiO_2 also controls the tribocorrosion of implants in orthopedics through the formation of passive layer on their surface (He et al., 2008; Ramalingam, Muralidharan, & Subramania, 2009). However, because of toxicological aspects, the biomedical application of pure nano-TiO_2 is a critical issue. Generally, particle size, specific surface area (SSA), chemical composition, structural property and solubility are vital in determining the toxicity of nanoparticles (Singh et al., 2007). Moreover, dosage, root of administration and transport of nano-TiO_2 are also associated with toxic potential (Kroll et al., 2011; Singh et al., 2007; Wu, 2010). Hence, we focused on how to overcome these adverse effects of TiO_2 by preparing a composite with biocompatible polymers such as chitosan, collagen poly(caprolactone) (PCL), poly(lactic acid) (PLLA) and sodium alginate (Luo, Wang, Xu, & Wang, 2009).

Among the widely recognized natural polymers, chitosan occupies a unique place due to its favorable biological properties, such as presence of free amino and hydroxyl functional groups; non-toxic, biodegradable nature; bacteriostatic properties; abundance in nature and structural similarity with extracellular matrix (Muzzarelli, 2010; Wang, de Boer, & de Groot, 2004). In addition, its hydrophilic surface promotes attachment and differentiation of osteoprogenitor cells (Zhang & Zhang, 2004; Luo et al., 2009; Muzzarelli, 2009). Moreover, it can be degraded in the human body by enzymes such as chitosanase and lysozyme (Yuan, Chesnutt, Wright, Haggard, & Bumgardner, 2008). However, less mechanical property and rapid degradability (Zhang & Zhang, 2004) limit wide use of chitosan in the biomedical field.

The defects of organic (chitosan) and inorganic (TiO_2) materials in biomedical application are overcome by the production of organic–inorganic nanocomposites with modified beneficial synergetic properties (Rani et al., 2011). These composites serve as a functional analog of natural material in the body (Amin & Panhuis, 2012). The formation of TiO_2–chitosan nanocomposites increases their mechanical property and antibacterial activity against bone infectants, and prevents the transport and accumulation of TiO_2 in the body (Ghosh, Bandyopadhyay, & Mukherjee, 2010) besides

* Corresponding author. Tel.: +91 4288 274741 4; fax: +91 4288 274880 (Direct)x274860.
E-mail addresses: kkavitha07@gmail.com (K. Kavitha), suthaasridhar@gmail.com (S. Sutha), prabhubpt16@gmail.com (M. Prabhu), veerajendran@gmail.com, directorrd@ksrct.ac.in (V. Rajendran), tjk@igcar.gov.in (T. Jayakumar).

0144-8617/$ – see front matter © 2012 Elsevier Ltd. All rights reserved.
http://dx.doi.org/10.1016/j.carbpol.2012.12.031

sustaining the degradation rate and release of ions (Ozerin et al., 2006).

Compared with the conventional synthesis method (blending) of TiO_2–chitosan nanocomposite (Ozerin et al., 2006), *in situ* sol–gel mediated synthesis produces homogenous dispersion of particles with strong interaction (Vona et al., 2007), thus enhancing the physicochemical properties and long-term functionalities (Al-Sagheer & Merchant, 2011; Yang, Li, Jiang, Lu, & Chen, 2009). Nevertheless, the biomedical application of TiO_2–chitosan nanocomposite, especially optimal concentration is a thrust area of current research. In this regard, *in situ*-synthesized biodegradable TiO_2–chitosan nanocomposites were analyzed for biological behavior. To the best of our knowledge, no report has been published about the combined properties of bioactivity, antibacterial activity and biocompatibility of such biodegradable materials, particularly *in situ*-synthesized TiO_2–chitosan nanocomposites.

The objective of this work was to synthesize the TiO_2–chitosan nanocomposites by *in situ* sol–gel process with different concentrations of chitosan. The nanocomposite powders were characterized using conventional techniques. Series of TiO_2–chitosan nanocomposites were analyzed through *in vitro* study to explore the bioactivity, antibacterial activity and cytotoxicity.

2. Materials and methods

2.1. Materials

Titanium isopropoxide ($Ti(OC_3H_7)_4$, 97%, Catalog No.: 205273, Sigma–Aldrich) isopropyl alcohol ($CH_3CHOHCH_3$, 99%), acetyl acetone ($C_5H_8O_2$, 98%) and nutrient media (all of analytical grade) purchased from Merck, Mumbai were used in this study. Chitosan, from crab shells (Catalog No.: 41,796-3), Dulbecco's modified Eagle's medium/Ham′s nutrient mixture of F12 (DMEM/F-12Ham, Catalog No.: 56498), and MTT (3-(4,5-dimethylthiazole-2-yl)-2,5-diphenyl tetrazolium bromide) kit (Catalog No.: 070M61471) were used as received from Sigma–Aldrich (USA).

2.2. Preparation of TiO_2–chitosan nanocomposites

TiO_2–chitosan nanocomposites with five different chitosan ratios (2:*x*, where *x* = 0.12, 0.25, 0.5, 1 and 2 (v/v); hereafter termed as T-C0.12, T-C0.25, T-C0.5, T-C1 and T-C2, respectively) were synthesized using modified *in situ* sol–gel method proposed by Yang et al. (2009) at room temperature. Titanium isopropoxide was diluted with isopropyl alcohol followed by the addition of acetyl acetone (to control hydrolysis) in the molar ratio 1:4:0.7. After 1 h, chitosan was dissolved in 2% acetic acid at different concentrations (0.12, 0.25, 0.5, 1 and 2 g/L). Thus prepared solutions were then added drop wise to dilute titanium isopropoxide separately under vigorous stirring. At certain point, the solutions turned into semisolid that were then dried at 433 K for 2–3 h to evaporate the solvent. The dried powders were ground and stored in desiccators to avoid agglomeration.

2.3. Characterization

The prepared TiO_2–chitosan nanocomposites were characterized by conventional techniques. The crystalline nature and structure of the nanocomposites were analyzed using X-ray diffractometer (XRD) (X'Pert Pro; PANalytical, the Netherlands) with Cu Kα as the radiation source (λ = 0.15406 Å). From the XRD peaks, the average crystalline size was calculated using Scherrer formula. Fourier transform infrared spectrometer (FTIR) (Spectrum 100; PerkinElmer, USA) was used to record the spectra at 300 K to confirm the occurrence of functional groups. The surface morphology and elemental compositions of the prepared nanocomposites were examined using techniques such as scanning electron microscopy combined with energy dispersive X-ray spectroscopy (SEM–EDX) (JSM-6390LV, Japan) and X-ray fluorescence spectrometry (XRF) (EDX-720; Shimadzu, Japan). The primary particle size was estimated using transmission electron microscopy (TEM) (CM200; Philips, USA). The SSA was measured using the Brunauer–Emmett–Teller analyzer (Autosorb AS-1MP; Quantachrome, USA). Total pore volume and average pore diameter of the prepared nanocomposites were calculated using the Brunauer–Joyner–Halenda method.

2.4. Antibacterial activity

Clinical isolates of bone-infecting organisms such as *Staphylococcus aureus* (ATCC 25923), *Escherichia coli* (ATCC 25922), *Klebsiella pneumoniae* (ATCC 13883) and *Bacillus subtilis* (ATCC 6051) were collected from the Microbial Type Culture Collection and Gene Bank, Chandigarh, India and were used to study the antibacterial effect of the prepared nanocomposites. Slants of above bacteria were cultured in 2 mL nutrient broth overnight, which were then transferred to 100 mL nutrient broth and incubated at 310 K for 3–4 h. Freshly grown cell suspension (0.1 mL) was uniformly swabbed onto a nutrient agar plate. In disk diffusion method, 50 mg of each sample was loaded on sterile disk and placed on the plate and incubated at 310 K for 24 h.

2.5. In vitro bioactivity

The 1.5 SBF solution was prepared using the standard procedure (Gerhardt, Jell, & Boccaccini, 2007; Kokubo & Takadama, 2006) with analytical grade chemicals and used in this study to explore the *in vitro* bioactivity of the prepared samples. Samples were immersed in 1.5 SBF solutions in the ratio of 1.5 g/L and incubated for 21 days at 310 ± 1 K. The ion exchange between the SBF and sample was recorded using pH and conductivity probes of 5-Star (Thermo Orion, USA). After incubation, the dry weight of the pellets was measured and compared with their initial weight. Hydroxyapatite (HAp) layer formation was confirmed by XRD, FTIR and XRF studies.

2.6. Swelling study

To explore the swelling behavior of the prepared nanocomposites, we measured the initial weight of the samples and then immersed them in phosphate-buffered saline (PBS) containing bottle (pH 7.4 at 310 ± 1 K) and incubated them for 7 days (Rani et al., 2011; Teodor, Simona Carmen, Petcu, Mihalache, & Somoghi, 2009). At defined days (1, 4 and 7), the buffer was carefully removed using filter paper and the wet weight was measured. The swelling ratio was calculated using the following equation:

$$W(\%) = \frac{W_w - W_0}{W_0} \times 100 \quad (1)$$

where W is the swelling ratio of the sample, W_0 the initial weight of the sample and W_w the wet weight of the PBS immersed sample.

2.7. Cell culture and cytotoxicity

AGS cell line (ATCC-1739) was purchased from the National Centre for Cell Science (Pune, India). The cells were allowed to grow in DMEM/F12Ham medium containing 10% fetal bovine serum, sodium pyruvate, 0.15% sodium bicarbonate, non-essential amino acids, 2 mM glutamine, penicillin (100 μg/mL) and streptomycin (100 μg/mL). AGS cell line is a suitable primary *in vitro* model to explore the toxicity of the nanoparticles. The viability of the cells was determined using the colorimetric MTT assay (Ghosh

et al., 2010). At 80–90% confluency, the cells were seeded into 96-well micro-titrate plate at a density of 1×10^3 cells per well and then allowed to adhere for 24 h. Filter-sterilized TiO_2–chitosan nanocomposites (T-C0.12, T-C0.25, T-C0.5, T-C1 and T-C2) were loaded into the wells with three concentrations, namely 1, 5 and 20 μg/mL, and incubated at 310 K for 48 h. Using inverted tissue culture binocular microscope, we observed the morphological changes of AGS cell lines for every 12 h. MTT solution (80 μg/mL) was added and the solution was incubated for 4 h, to reduce it and to form the formazan crystals. These crystals were dissolved in dimethyl sulfoxide. During the process, the color of the solution changed from yellow to pink. The optical intensity (OD) was read at 570 nm with 630 nm as the reference. The percentage of cell viability was calculated using the following formula:

$$\frac{\text{OD of the nanoparticle treated cells}}{\text{OD of the control cells}} \times 100 \quad (2)$$

2.8. Statistical analysis

To determine cell viability, we performed the experiment in triplicate and represented data as mean ± standard deviation. Cell viability (%) of all five prepared TiO_2–chitosan nanocomposites with three different concentrations was compared with that of the untreated cells and analyzed using one-way analysis of variance followed by Tukey's least significant difference and Duncan's *post hoc* tests. Statistical analyses were done using SPSS software, version 16.0. Statistical significance was considered at 5% level ($p < 0.05$) along with the untreated AGS cell lines.

3. Results and discussion

The XRD patterns of different ratios of TiO_2–chitosan nanocomposites in the range of $2\theta = 10$–80° are shown in Fig. 1. As indicated in Fig. 1(a), all the diffraction peaks are indexed and agree well with the tetragonal anatase phase of TiO_2 (JCPDS file no. 21-1276). Further, the absence of any other characteristic peaks indicates high purity of the powder. The chitosan inclusion in TiO_2 does not induce any peak shift. However, a reduction in the peak intensity is observed with respect to the higher concentration of chitosan. By applying the Scherrer equation (Sun, Sun, Zhang, & Wang, 2008) on the obtained XRD strong (1 0 1) plan, the average crystallite size is calculated and shown in Table 1. The addition of chitosan to TiO_2 decreases the crystallite size and crystalline nature.

Fig. 2(a) shows the infrared transmittance spectra in the range of 2500–400 cm^{-1} for the prepared samples. The obtained characteristic peaks at 900–400, 1029, 1152 and 1370–1450 cm^{-1} reveals respectively for Ti–O–Ti stretching, bending mode of Ti–O–C, stretching bands of C–O–C and CH_3 stretching bands (Al-Sagheer & Merchant, 2011; Guo, Lin, Wang, & Song, 2003; Nakayama & Hayashi, 2007), which confirm the formation of TiO_2–chitosan composite. The presence of Ti–OH stretching at 1287 cm^{-1} is a constructive site for accumulation of ions and formation of HAp layer (Nakayama & Hayashi, 2007). C–N and C–N–H mode of chitosan is confirmed through the corresponding peak near 1528–1534 cm^{-1} (Zawadzki & Kaczmarek, 2010). Moreover, the corresponding amide II (NH) and amide I (C=O) bands of chitosan are also observed at 1637–1715 cm^{-1} (Zawadzki & Kaczmarek, 2010).

TEM images (Fig. 3) and Table 1 show the particle size of the nanocomposites with an average diameter of 20 nm. The primary particle size of the prepared TiO_2 (T-C0) is 10.58 nm. It is noteworthy that the particle size of the *in situ*-synthesized TiO_2 with different concentrations of chitosan, namely T-C0.12, T-C0.25 T-C0.5, T-C1 and T-C2, is 5.98, 5.87, 5.73, 5.23 and 4.50 nm, respectively. It reveals that the addition of chitosan progressively

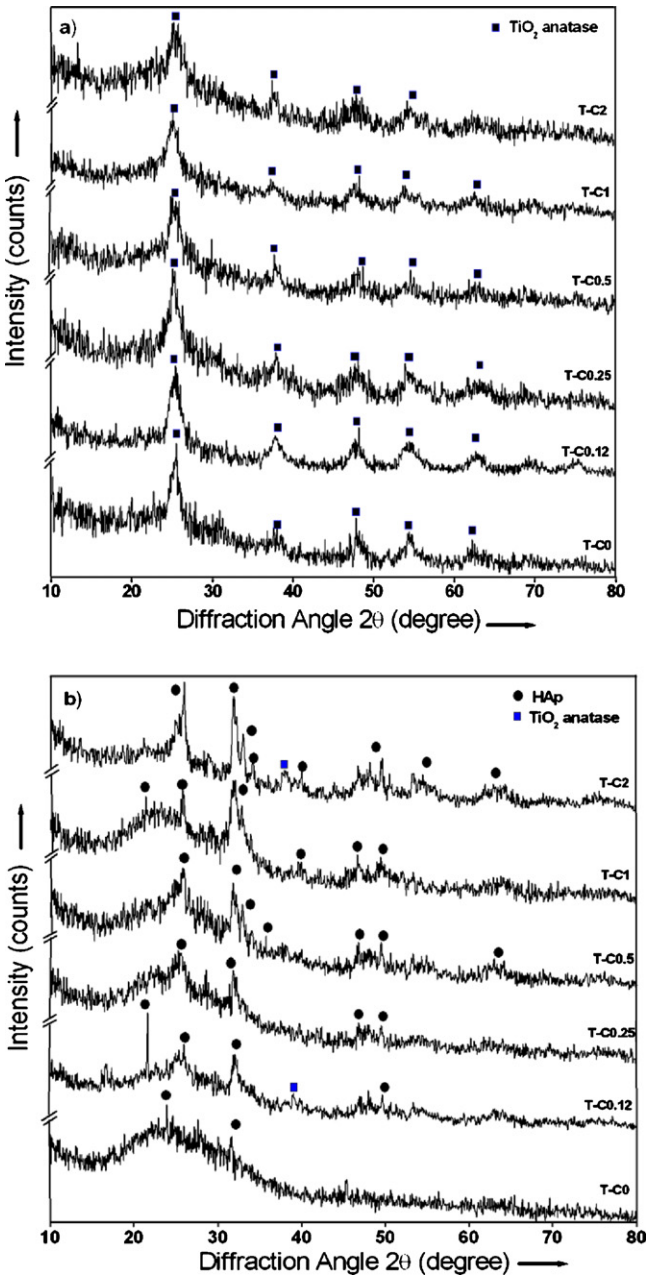

Fig. 1. X-ray diffraction pattern of a series of TiO_2–chitosan nanocomposite for bioactivity (a) before *in vitro* study and (b) after *in vitro* study.

decreases the particle size which allows absorption of more nutrients from the body (Rani et al., 2011). Electron diffraction patterns of the selected area of the samples are inserted in their respective TEM images. These observations show that the crystalline nature of TiO_2 is reduced as a result of high concentration of chitosan in the composite, which is well indexed with the XRD pattern.

The observed SEM image (Fig. 4) shows the presence of spherical and irregular shapes of TiO_2–chitosan nanocomposites with an average diameter of approximately 120 nm. The surface morphology of the prepared T-C0 sample shows the well-formed spherical shape. As the concentration of chitosan increases in the composite, it progressively changes the spherical shape of TiO_2 to the agglomerated irregular shape. In addition to morphology, the elemental compositions of prepared samples are defined from EDAX results.

The SSA of the prepared nanoparticles is 114.24, 214.73, 244.47, 265.33 and 237.71 m^2/g, respectively, for T-C0.12, T-C0.25, T-C0.5,

Table 1
Concentration of the chitosan and physicochemical properties of prepared TiO_2–chitosan nanocomposites.

Sample name	Concentration of chitosan (g/L)	Crystallite size (nm)	Particle size (nm)	Surface area (m^2/gm)	Total pore volume (cc/gm)	Average pore diameter (nm)
T-C0	0	3.60	10.58	208.41	0.0945	1.262
T-C0.12	0.125	3.58	5.98	114.24	0.0562	1.413
T-C0.25	0.25	3.22	5.87	214.73	0.1029	1.917
T-C0.5	0.5	3.00	5.73	244.47	0.1174	1.921
T-C1	1	2.13	5.23	265.33	0.130	1.966
T-C2	2	2.13	4.50	237.71	0.1150	1.936

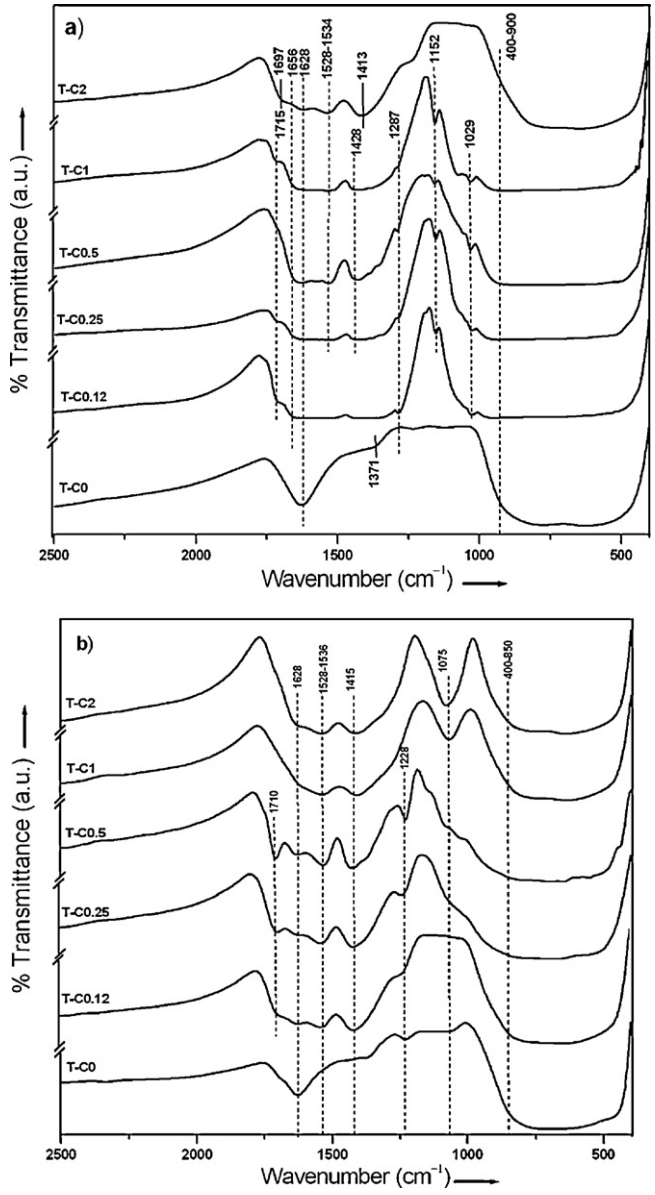

Fig. 2. Fourier transform infrared spectra of TiO_2–chitosan nanocomposites for bioactivity (a) before *in vitro* study and (b) after *in vitro* study.

T-C1 and T-C2 samples (Table 1). In addition, total pore volume and average pore diameter are calculated according to Barrett, Joyner, and Halenda (1951), as shown in Table 1. The higher surface area and pore size of the prepared nanocomposites help the cell growth during the implantation and tissue engineering. Table 1 shows that the increasing chitosan content in composites is directly proportional to the SSA, total pore volume and diameters. The SSA analysis of pure nano-TiO_2 (T-C0, 208 m^2/g) illustrates that the addition of chitosan has both adverse and constructive effects on SSA, depending on the concentration of chitosan. T-C1 is the optimal ratio of the composite to increase the SSA and to improve the interaction with cell.

3.1. Swelling study

The swelling percentages of the nanocomposites are calculated from the wet weight (310 ± 1 K) of the PBS immersed samples at three days interval and are given in Table 2. Previous studies show that the swelling avails to increase the pore size of the particles, thereby increasing the surface area and allowing absorption of more nutrients both *in vitro* and *in vivo* (Jayakumar et al., 2011; Rani et al., 2011). It could be observed from Table 2 that an increase in the chitosan content in the composite increases the swelling capacity. The observed swelling property is due to the presence of chitosan (Teodor et al., 2009). Thus, it increases the sample's probability of cell attachment and growth in a three-dimensional way (Jayakumar et al., 2011; Rani et al., 2011). No significant difference in swelling is observed on days 7 and 4. However, a notable difference is observed between days 1 and 4 (Table 2). This result shows the swelling capacity of the chitosan with respect to time. Both the samples T-C2 and T-C1 attain maximum swelling property respectively, as 42.84% and 42.89% on day 7. Further, it concludes that the composite has no significant changes in the swelling capacity above the ratio of 2:1 (T-C1), and TiO_2 controls the swelling capacity of chitosan.

3.2. Bioactivity study

Fig. 5 shows the pH and conductivity measurements of the nanocomposites in 1.5 SBF, both well correlated with each other with respect to the ionic changes. All the samples have same pattern of exchange of ions in 1.5 SBF, besides a slight increase in pH at the higher concentration of chitosan. After soaking the samples in 1.5 SBF, a sudden decrease in pH and increase in conductivity is observed due to the solubility of the samples (Murugan & Ramakrishna, 2005). A continuous exchange of ions is observed till day 18 while a sharp decrease in conductivity and increase in pH is observed up to day 12, which is due to the more absorption of supplementary ions and sufficient use of OH^- ions from the 1.5 SBF solution to initiate the formation of HAp layer on the surface of the samples. Both pH and conductivity measurements attain stationary phase after day 18. This may be due to the saturation of ion deposition on the sample. Moreover, on day 21, both pH and conductivity measurements are increased slightly due to the release of excess ions from the surface of the samples after the formation of HAp layer. The observed results confirm that these kind of pH measurements (ion exchanges) in the prepared samples are favorable for the formation of HAp layer (Saravanakumar, Rajkumar, & Rajendran, 2011). Specially, the analysis of T-C2 and T-C1 samples reveals good exchange of ions.

The powders collected after the 1.5 SBF incubation show four distinct diffraction peaks at 21.8, 25.3, 25.8 and 31.7° correspond respectively, to (2 0 0), (2 0 1), (0 0 2) and (2 1 1) plan, which indicates the reflection of HAp layer formation (JCPDS file no. 090432;

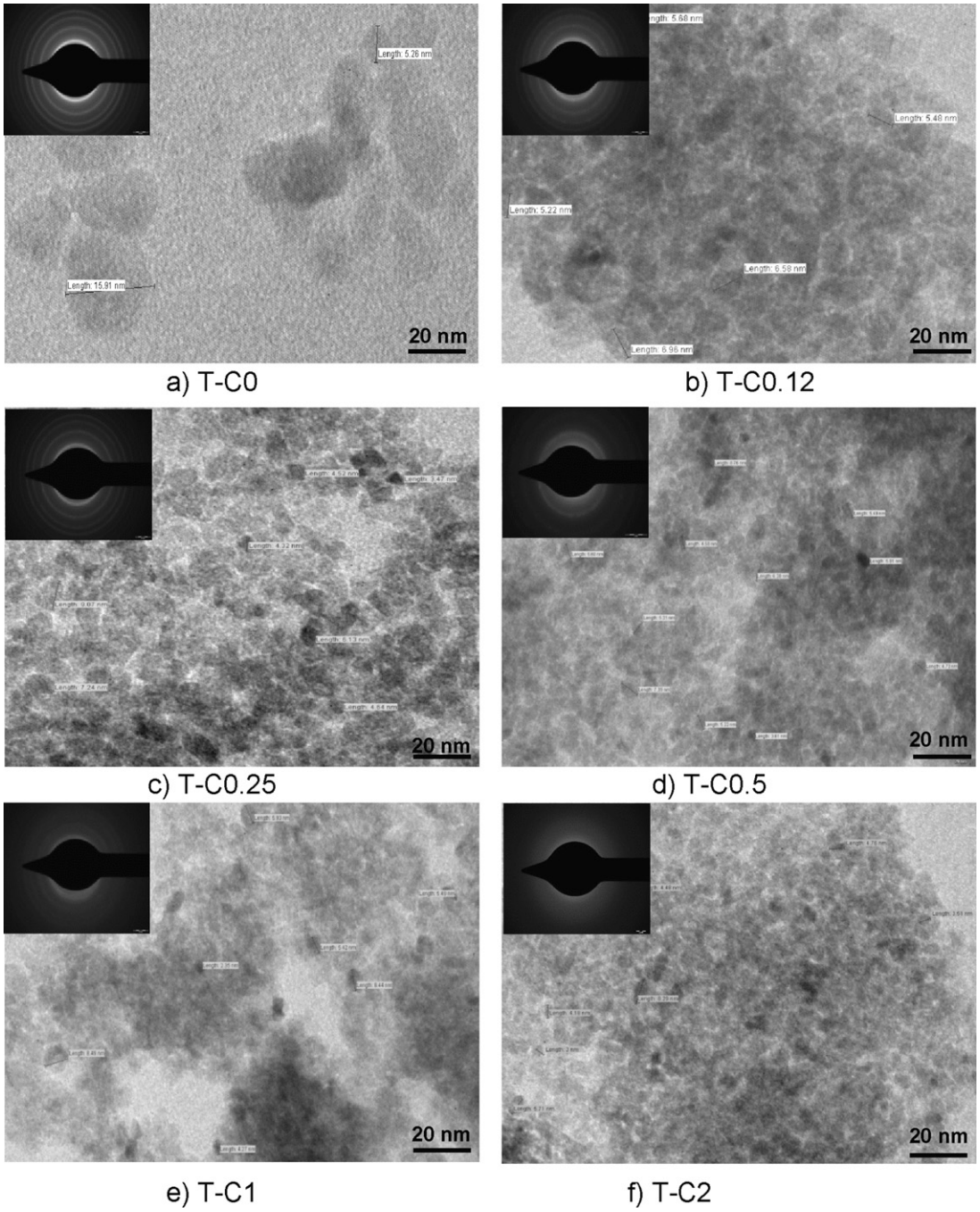

Fig. 3. Transmission electron microscopic images and corresponding diffraction pattern of prepared TiO_2–chitosan nanocomposites.

Table 2
In vitro bioactivity, swelling capacity and antibacterial activity of TiO_2–chitosan nanocomposites.

Sample name	After *in vitro* 1.5 SBF study			Swelling weight in PBS			Zone of inhibition in *S. aureus* (mm)
	Ca/P ratio (%)	Weight modulations (%)	Crystallite size (nm)	1st day (%)	4th day (%)	7th day (%)	
T-C0	1.732	−2.51	17.53	19.02	10.32	12.90	0
T-C0.12	1.750	2.70	68.67	22.89	29.32	29.16	0
T-C0.25	1.712	1.95	88.09	28.02	31.95	30.24	5
T-C0.5	1.622	1.57	21.628	30.75	37.74	37.80	10
T-C1	1.5796	1.41	61.77	36.14	42.82	42.89	14
T-C2	1.474	1.22	57.68	35.32	42.83	42.84	16

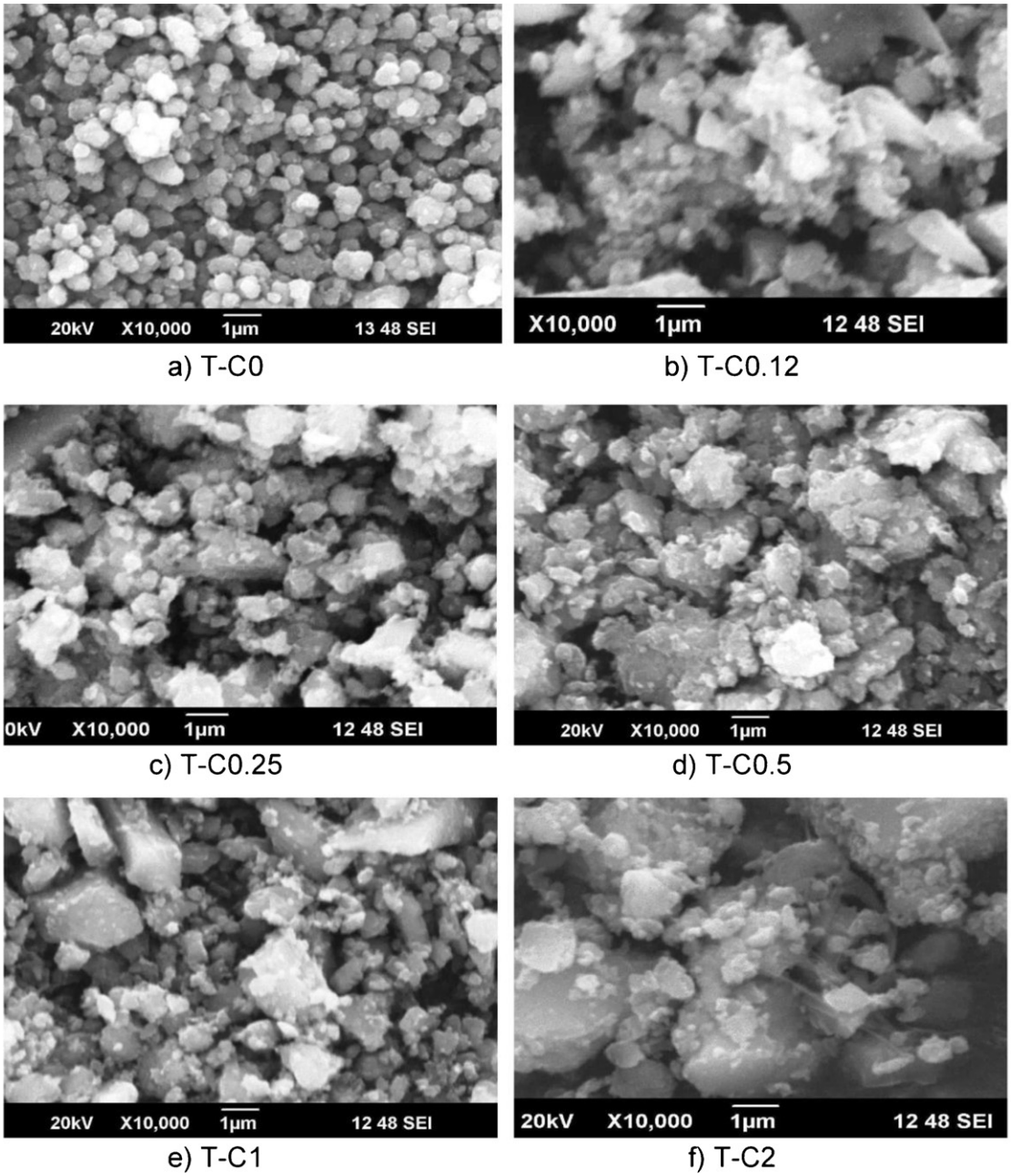

Fig. 4. Scanning electron microscopic images of TiO_2–chitosan nanocomposites.

Fig. 1(b)). The absence of any other characteristic peaks indicates domination of well-formed crystalline HAp. An irregular increase in crystallite size is observed after the immersion in SBF (Table 2), which is due to the agglomeration of TiO_2, swelling behavior of chitosan and the formation of apatite layer. When chitosan concentration is increased from 0% to 2%, the increase in the number of HAp crystalline peaks and a gradual diminutive peak shift of HAp are observed toward the lower diffraction angle. This is because of lower particle and crystallite sizes. The well-formed HAp layer indicates the bioactivity of the samples.

Fig. 2(b) shows the IR spectra of the samples immersed in 1.5 SBF for 21 days. The observed broad Ti–O–Ti peak slightly sharpened and the Ti–O–C band is shifted slightly toward left-hand side compared with the one shown in Fig. 2(a). The characteristic peak observed at 1415 cm^{-1} corresponds to CO_3^{2-} due to the formation of HAp layer (Siriphannon, Kameshima, Yasumori, Okada, & Hayashi, 2002), which is clearly observed in the samples containing higher chitosan content. The other characteristic peaks remain same as shown in Fig. 2(a). This result confirms that the phosphate bands are dominated by the broad absorption peak of titanium bands (400–900 cm^{-1}), as reported earlier (Dai et al., 2010; Thomas et al., 2007).

After *in vitro* study, the dry weight of the 21-day old samples is compared with the initial weight and weight loss is shown in Table 2. After *in vitro* bioactivity study, all TiO_2 samples containing chitosan show an increase in their weight except for the pure TiO_2, which is due to their swelling capacity during the initial (Teodor et al., 2009). Moreover, the weight modulations imply the degradation ability of the powders. In contrast, the observed increase in weight percentage of the samples containing low chitosan concentration is due to the slow swelling, thereby interrupting degradation. Swelling percentage and weight loss

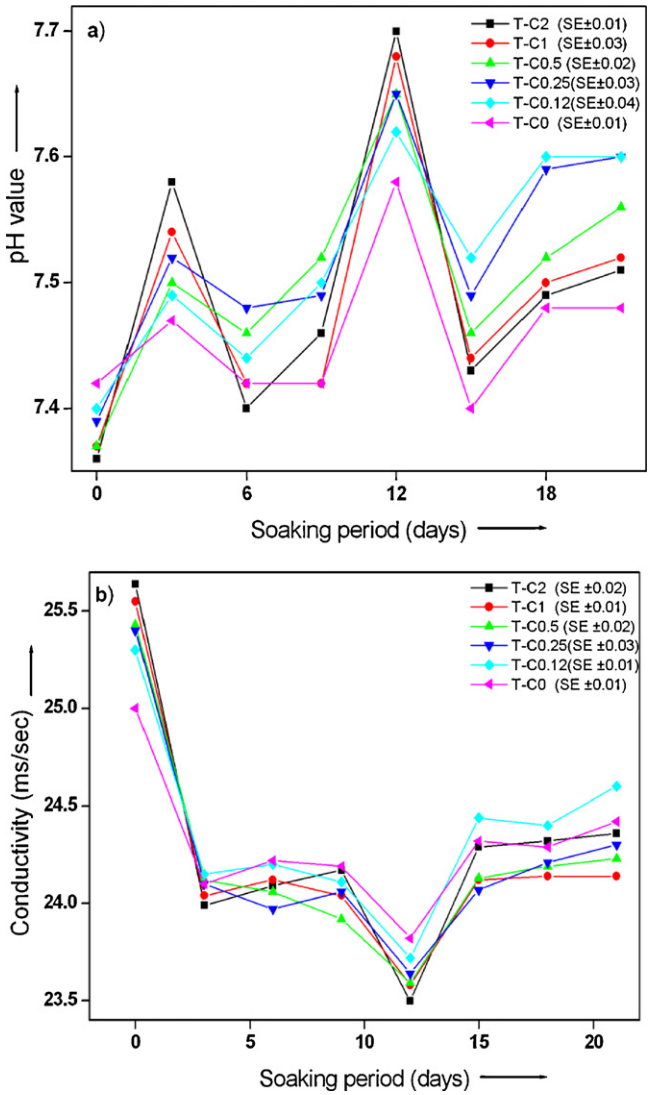

Fig. 5. Measurements of ionic exchanges between 1.5 SBF solution and TiO_2–chitosan (1.5 g/L) nanocomposites (a) pH *vs.* soaking period and (b) conductivity during *in vitro* bioactivity.

(Table 2) of the prepared nanoparticles collectively reveal that the exponential swelling behavior is observed at the initial days. After attaining the equilibrium, it starts degrading gradually in the SBF solution. Composite having higher chitosan content leads to high swelling property. The addition of nano-TiO_2 controls the swelling property gradually with chitosan concentration (Jayakumar et al., 2011; Rani et al., 2011). The swelling property of the nanoparticles is directly proportional to the degradation rate (Rani et al., 2011) which is in close agreement with our T–C samples. The *in situ*-synthesized TiO_2–chitosan nanocomposites reveal a strong interaction and good network-forming ability with each other, thereby facilitating the favorable swelling and degradation rate (Al-Sagheer & Merchant, 2011).

The presence of calcium and phosphate on the surface of the sample is measured by XRF. The Ca/P ratio is calculated for all the samples and is given in Table 2. It is known that the formation of HAp layer mainly depends on the Ca/P ratio (Choi & Kumta, 2006). Table 2 infers that the prepared TiO_2–chitosan composite facilitates a better formation of HAp layer than the pure TiO_2. Samples having less concentration of chitosan and pure TiO_2 (T-C0.12, T-C0.25 and T-C0) show carbonate-substituted HAp (Ca/P ratio = 1.67–1.93), whereas samples T-C0.5 and TA-C1 form the oxy-HAp (Ca/P ratio = 1.5–1.67) (Rajkumar, Meenakshi Sundaram, & Rajendran, 2011). However, sample T-C2 shows a calcium-deficient HAp formation (Ca/P ratio = 1.2–1.56). Interestingly, the Ca/P ratio decreases when the chitosan content is increased from 0 to 2 g. It indicates that the increase in chitosan content reduces the absorption of calcium and *vice versa* in phosphate. It is well known that oxy-HAp is an appropriate ratio of accepted stoichiometry for bone (Yan, Li, Deng, Zhuang, & Sun, 2001). The samples containing 0.5 and 1 g chitosan (T-C0.5 and T-C1) are the more appropriate composites for bone-forming HAp.

3.3. Antibacterial activity

The antibacterial activity of prepared TiO_2–chitosan nanocomposites are screened against *S. aureus*, *E. coli*, *K. pneumoniae* and *B. subtilis*. No marked antibacterial activity is found in *E. coli*, *K. pneumoniae* and *B. subtilis* whereas a gradual increase in inhibition is observed in *S. aureus* at higher chitosan concentration (Table 2). Pure nano-TiO_2-impregnated disk does not show any zone of inhibition; however, TiO_2–chitosan nanocomposite shows an inhibition in the same concentration. Chitosan is capable of forming the layer on the surface of cell wall and preventing the nutrient transport, thereby inhibiting the growth of bacteria (Amin & Panhuis, 2012; Lim, Wang, Shi, Poh, & Neoh, 2009). The inhibition

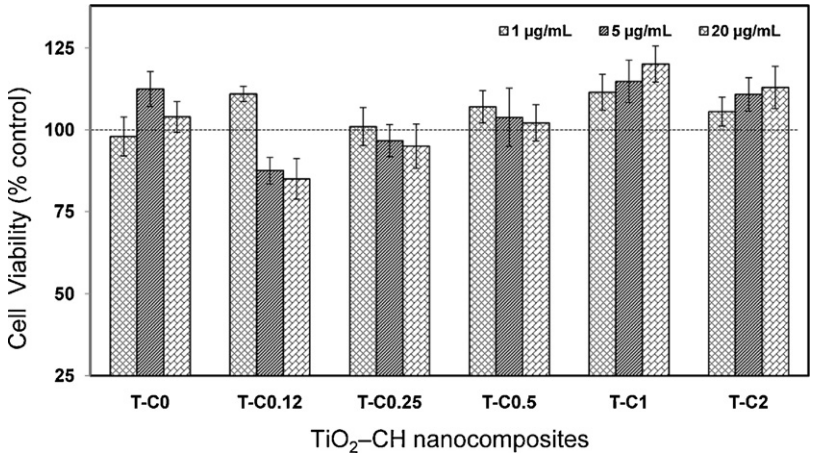

Fig. 6. Cytotoxicity test of prepared TiO_2–chitosan nanocomposites using MTT assay.

depends on the physicochemical properties and the concentration of the sample (Amin & Panhuis, 2012). These surface characteristics of the bacterial cell wall also have an important role in antibacterial activity (Chung et al., 2004). This study confirms that the TiO_2–chitosan nanocomposites support prevention of the growth of *S. aureus*, especially at higher chitosan concentration (T-C2) (Table 2). This property is due to the above mentioned antibacterial activity of chitosan and appropriate interaction of nanoparticles with the cell walls.

3.4. Cytotoxicity tests

In vitro cytotoxicity assay is carried out in triplicates on AGS cells line with three different concentrations of the prepared nanoparticles, namely 1, 5 and 20 μg/mL. No significant phenotypic changes are observed after 48 h of the nanoparticle treatment. The biocompatibility experiment concerns cytotoxicity of the prepared samples and is performed using MTT assay. The percentage of cell viability is increased in T-C1 (1 g chitosan) than at any other concentration. However, in the samples containing too high (T-C2) and too low (T-C0.12 and T-C0.25) chitosan concentration and pure nano-TiO_2 (T-C0), the cell viability decreases with megre amount of cell death (Fig. 6). The cell death and increased cell viability in T-C1 are caused by the properties, such as surface/volume ratio, swelling capacity and appropriate interface layer formation (HAp), of the nanoparticles. As observed from Fig. 6, high concentration of sample treatment (20 μg/mL) in AGS cell line decreases the cell viability from T-C0 to T-C0.5, whereas in T-C1 and T-C2, nanostructures are highly biocompatible in all the concentration of treatments. It also implies that T-C1 is the optimal material for cell viability than T-C2 because of its high surface area/volume ratio and ideal reactivity with surface of cell wall (Saquib et al., 2012). The results of both statistical analyses and MTT assay show that there is no significant cytotoxicity of the prepared nanocomposites in AGS cell line.

4. Conclusions

TiO_2–chitosan nanocomposites are synthesized at five different concentrations by *in situ* method. The prepared nanocomposites are characterized to explore the crystalline nature, functional groups, bonding pattern, particle size, SSA and morphology. These nanocomposites resolve the adverse effects of TiO_2 and the complication of chitosan in the biomedical field. The smaller particle size of TiO_2–chitosan increases the absorption of nutrients from the body and helps the formation of an apatite layer through the conventional principles of surface/volume ratio. In addition, composites with 114.24 –265.33 m^2/g range of specific surface area and controlled swelling property leads to improve the cell attachment and avoid the transport and agglomeration of the particles in the body. The increase in chitosan content from T-C0 to T-C2 leads to an increase in antibacterial activity and ionic exchange of TiO_2–chitosan composites in the 1.5 SBF solution. However, the swelling property, cytotoxicity and elemental composition of composites in the 1.5 SBF study reveal that the sample T-C1 (2:1) is an optimal composite for biomedical application due to the appropriate stoichiometric ratio than the sample T-C2 (2:2). This study concludes that T-C1 is the optimal material that possesses high potential, such as biomimic, bioactive and biocompatible nature, and thus it is more suitable to the requirements of bone reconstruction, regeneration and tissue engineering.

Acknowledgements

The authors would like to acknowledge the UGC–DAE–Consortium for Scientific Research, Kalpakkam and Dr. G. Amarendra, Head, Metal Physics Section, Indira Gandhi Center for Atomic Research, Kalpakkam node for the financial support and valuable suggestions to carry out this research project (CSR/Acctts/2010–11/1136 dt.06.01.2011). The authors are thankful to Dr. G. Kumaresan and Mr. P. Jayaprakash, Department of genetics, School of biological sciences, Madurai Kamaraj University for their technical support in the toxicity studies.

References

Al-Sagheer, F. A., & Merchant, S. (2011). Visco-elastic properties of chitosan–titania nano-composites. *Carbohydrate Polymers*, *85*, 356–362.
Amin, K. A. M., & Panhuis, M. I. H. (2012). Reinforced materials based on chitosan, TiO_2 and Ag composites. *Polymers*, *4*(1), 590–599.
Barrett, E. P., Joyner, L. G., & Halenda, P. P. (1951). The determination of pore volume and area distributions in porous substances. *Journal of the American Ceramic Society*, *73*, 373–380.
Choi, D., & Kumta, P. N. (2006). An alternative chemical route for the synthesis and thermal stability of chemically enriched hydroxyapatite. *Journal of the American Ceramic Society*, *89*, 444–449.
Chung, Y. C., Su, Y. P., Chen, C. C., Jia, G., Wang, H. L., Wu, J. C. G., et al. (2004). Relationship between antibacterial activity of chitosan and surface characteristics of cell wall. *Acta Pharmacologica Sinica*, *25*(7), 932–936.
Dai, S., Wu, Y., Sakai, T., Du, Z., Sakai, H., & Abe, M. (2010). Preparation of highly crystalline TiO_2 nanostructures by acid-assisted hydrothermal treatment of hexagonal-structured nanocrystalline titania/cetyltrimethyl ammonium bromide nanoskeleton. *Nanoscale Research Letters*, *5*, 1829–1835.
Gerhardt, L. C., Jell, G. M. R., & Boccaccini, A. R. (2007). Titanium dioxide (TiO_2) nanoparticles filled poly(D,L lactid acid) (PDLLA) matrix composites for bone tissue engineering. *Journal of Material Science Materials in Medicine*, *18*, 1287–1298.
Ghosh, M., Bandyopadhyay, M., & Mukherjee, A. (2010). Genotoxicity of titanium dioxide (TiO_2) nanoparticles at two trophic levels: Plant and human lymphocytes. *Chemosphere*, *81*, 1253–1262.
Guo, W., Lin, Z., Wang, X., & Song, G. (2003). Sonochemical synthesis of nanocrystalline TiO_2 by hydrolysis of titanium alkoxides. *Microelectronic Engineering*, *66*, 95–101.
He, G., Hua, J., Wei, S. C., Li, J. H., Liang, X. H., & Luo, E. (2008). Surface modification of titanium by nano-TiO_2/HA bioceramic coating. *Applied Surface Science*, *255*, 442–445.
Hua, D., Cheuk, K., Wei-ning, Z., Chen, W., & Chang-fa, X. (2007). Low temperature preparation of nano TiO_2 and its application as antibacterial agents. *Transactions of Nonferrous Metals Society of China*, *17*, s00–s703.
Isikli, C., Hasirci, V., & Hasirci, N. (2012). Development of porous chitosan–gelatin/hydroxyapatite composite scaffolds for hard tissue-engineering applications. *Journal of Tissue engineering and Regenerative Medicine*, *6*(2), 135–343.
Jayakumar, R., Ramachandran, R., Divyarani, V. V., Chennazhi, K. P., Tamura, H., & Nair, S. V. (2011). Fabrication of chitin–chitosan/nano TiO_2-composite scaffolds for tissue engineering applications. *International Journal of Biological Macromolecules*, *48*(2), 336–344.
Kokubo, T., & Takadama, H. (2006). How useful is SBF in predicting in vivo bone bioactivity? *Biomaterials*, *27*(15), 2907–2915.
Kroll, A., Dierker, C., Rommel, C., Hahn, D., Wohlleben, W., Schulze-Isfort, C., et al. (2011). Cytotoxicity screening of 23 engineered nanomaterials using a test matrix of ten cell lines and three different assays. *Particle and Fibre Toxicology*, *8*, 9.
Lim, T. Y., Wang, W., Shi, Z., Poh, C. K., & Neoh, K. G. (2009). Human bone marrow-derived mesenchymal stem cells and osteoblast differentiation on titanium with surface-grafted chitosan and immobilized bone morphogenetic protein–2. *Journal of Materials Science: Materials in Medicine*, *20*(1), 1–10.
Luo, Y. B., Wang, X. L., Xu, D. Y., & Wang, Y. Z. (2009). Preparation and characterization of poly(lactic acid)-grafted TiO_2 nanoparticles with improved dispersions. *Applied Surface Science*, *255*, 6795–6801.
Murugan, R., & Ramakrishna, S. (2005). Aqueous mediated synthesis of bioresorbable nanocrystalline hydroxyapatite. *Journal of Crystal Growth*, *74*, 209–213.
Muzzarelli, R. A. A. (2009). Chitins and chitosans for the repair of wounded skin, nerve cartilage and bone. *Carbohydrate Polymers*, *76*, 167–182.
Muzzarelli, R. A. A. (2010). Chitins and chitosans as immunoadjuvants and non-allergenic drug carriers. *Marine Drugs*, *8*(2), 292–312.
Nakayama, N., & Hayashi, T. (2007). Preparation and characterization of poly(L-lactic acid)/TiO_2 nanoparticle nanocomposite films with high transparency and efficient photodegradability. *Polymer Degradation and Stability*, *92*, 1255–1264.
Ozerin, A. N., Zelenetskii, A. N., Akopova, T. A., Pavlova-Verevkina, O. B., Ozerina, L. A., Surin, N. M., et al. (2006). Nanocomposites based on modified chitosan and titanium oxide. *Polymer Science Series A*, *48*(6), 638–643.
Rajkumar, M., Meenakshi Sundaram, N., & Rajendran, V. (2011). Preparation of size controlled, stoichiometric and bioresorbable hydroxyapatite nanorod by varying initial pH Ca/P ratio and sintering temperature. *Digest Journal of Nanomaterials and Biostructures*, *6*, 169–179.

Ramalingam, S., Muralidharan, V. S., & Subramania, A. (2009). Electrodeposition and characterization of Cu–TiO_2 nanocomposite coatings. *Journal of Solid State Electrochemistry*, *13*, 1777–1783.

Rani, V. V. D., Ramachandran, R., Chennazhi, K. P., Tamura, H., Nair, S. V., & Jayakumar, R. (2011). Fabrication of alginate/nano TiO_2 needles composite scaffolds for tissue engineering applications. *Carbohydrate Polymers*, *83*, 858–864.

Saquib, Q., Al-Khedhairy, A. A., Siddiqui, M. A., Tarboush, F. M. A., Azam, A., & Musarrat, J. (2012). Titanium dioxide nanoparticles induced cytotoxicity oxidative stress and DNA damage in human amnion epithelial (WISH) cell. *Toxicology in Vitro*, *26*, 351–361.

Saravanakumar, B., Rajkumar, M., & Rajendran, V. (2011). Synthesis and characterization of nanobioactive glass for biomedical applications. *Materials Letters*, *65*(1), 31–34.

Singh, S., Shi, T., Duffin, R., Albrecht, C., Berlo, D. V., Hohr, D., et al. (2007). Endocytosis oxidative stress and IL-8 expression in human lung epithelial cells upon treatment with fine and ultrafine TiO_2: Role of the specific surface area and of surface methylation of the particles. *Toxicology and Applied Pharmacology*, *222*, 141–151.

Siriphannon, P., Kameshima, Y., Yasumori, A., Okada, K., & Hayashi, S. (2002). Formation of hydroxyapatite on $CaSiO_3$ powders in simulated body fluid. *Journal of the European Ceramic Society*, *22*, 511–520.

Sun, S. Q., Sun, B., Zhang, W., & Wang, D. (2008). Preparation and antibacterial activity of Ag-TiO_2 composite film by liquid phase deposition (LPD) method. *Bulletin of Materials Science*, *31*(1), 61–66.

Teodor, E., Simona Carmen, L., Petcu, C., Mihalache, M., & Somoghi, R. (2009). Nanostructured biomaterials with controlled properties synthesis and characterization. *Nanoscale Research Letters*, *4*, 544–549.

Thomas, V., Dean, D. R., Jose, M. V., Mathew, B., Chowdhury, S., & Vohra, Y. K. (2007). Nanostructured biocomposite scaffolds based on collagen coelectrospun with nanohydroxyapatite. *Biomacromolecules*, *8*, 631–637.

Vona, M. L. D., Ahmed, Z., Bellitto, S., Lenci, A., Traverse, E., & Licoccia, S. (2007). SPEEK–TiO_2 nanocomposite hybrid proton conductive membranes via *in situ* mixed sol–gel process. *Journal of Membrane Science*, *296*, 156–161.

Wang, J., de Boer, J., & de Groot, K. (2004). Preparation and characterization of electrodeposited calcium phosphate/chitosan coating on Ti_6Al_4V plates. *Journal of Dental Research*, *83*(4), 296–301.

Wu, Y. A. (2010). The assessment of cytotoxicity of organic/inorganic nanoparticles by cultured cell system. In *103rd A & WMA's annual conference and exhibition* Calgary, Alberta, Canada.

Yan, L., Li, Y., Deng, Z. X., Zhuang, J., & Sun, X. (2001). Surfactant-assisted hydrothermal synthesis of hydroxyapatite nanorods. *International Journal of Inorganic Materials*, *3*, 633–637.

Yang, D., Li, J., Jiang, Z., Lu, L., & Chen, X. (2009). Chitosan/TiO_2 nanocomposite pervaporation membranes for ethanol dehydration. *Chemical Engineering Science*, *64*, 3130–3137.

Yuan, Y., Chesnutt, B. M., Wright, L., Haggard, W. O., & Bumgardner, J. D. (2008). Mechanical property, degradation rate, and bone cell growth of chitosan coated titanium influenced by degree of deacetylation of chitosan. *Journal of Biomedical Materials Research Part B: Applied Biomaterials*, *86*(1), 245–252.

Zawadzki, J., & Kaczmarek, H. (2010). Thermal treatment of chitosan in various condition. *Carbohydrate Polymers*, *80*, 394–400.

Zhang, Y., & Zhang, M. (2004). Cell growth and function on calcium phosphate reinforced chitosan scaffolds. *Journal of Material Science Materials in Medicine*, *15*(3), 255–260.